IEEE Access
Multidisciplinary | Rapid Review | Open Access Journal

Received October 24, 2020, accepted November 3, 2020, date of publication November 16, 2020,
date of current version November 24, 2020.

Digital Object Identifier 10.1109/ACCESS.2020.3037557

An Improved Design of an Adaptive Sliding Mode Controller for Chattering Attenuation and Trajectory Tracking of the Quadcopter UAV

AHMED ELTAYEB[1], MOHD FUA'AD RAHMAT[1], (Senior Member, IEEE), MOHD ARIFFANAN MOHD BASRI[1], M.A MOHAMMED ELTOUM[2], AND SAMI EL-FERIK[2]

[1]School of Electrical Engineering, Universiti Teknologi Malaysia, Johor 81310, Malaysia
[2]Systems Engineering Department, King Fahd University of Petroleum and Minerals, Dhahran 31261, Saudi Arabia

Corresponding authors: Ahmed Eltayeb (ahmedtayeb5@gmail.com) and Mohd Fua'ad Rahmat (fuaad@fke.utm.my)

ABSTRACT Quadcopter unmanned aerial vehicles (UAVs) systems are receiving remarkable attention from researchers due to their daily use in numerous applications, particularly at the current time where UAVs are playing a significant role in combating the COVID-19 pandemic. This paper is concerned with the problem of UAV navigation and control in the presence of uncertainty and external disturbances. It addresses this issue by proposing an improved adaptive sliding mode control (IASMC). Improved control law generates an adaptive switching gain achieving fast adaptation and robustness against both parameter uncertainties and external disturbances. Simultaneously, the control law allows for maintaining robust trajectory tracking with chattering attenuation. The performance of the proposed IASMC controller has been evaluated using a Matlab/Simulink platform. The obtained simulation results showed that the proposed IASMC control scheme as an inner loop controller is robust when dealing with uncertainties and can effectively track the desired trajectories while significantly attenuating the well-known chattering introduced by the SMC controller.

INDEX TERMS Quadcopter UAV, PID controller, adaptive control, SMC control, type-2 fuzzy logic, chattering.

I. INTRODUCTION

Recently, quadcopter UAVs are receiving significant interest from researchers. The quadcopter UAV has been involved in numerous applications, particularly at the current time when it is playing a significant role in combating the COVID-19 pandemic, for example, monitoring the curfew process, spraying antiseptics in public and open areas, and being used in rescue and food delivery operations. These services reduce the spread of the COVID-19 virus, in addition to conventional applications in the military and other civilian sectors. Previously, quadcopter UAVs were mainly used for military purposes, however, over time they have gradually become involved in civilian applications such as traffic surveillance, photography, security, environmental monitoring, scientific research, agriculture, etc., [1].

Applications for the quadcopter are increasing rapidly, a fact which has motivated researchers to develop reliable and robust control algorithms to meet application requirements and perform the assigned tasks successfully. This work will focus on model-based control methods which consider the dynamics of the model in controller design stages.

Quadcopter control is a challenging task due to the high nonlinearity of its dynamics, coupling dynamics properties, unknown and unbounded parameters uncertainties, unknown disturbances, and unmodelled dynamics. These unwanted aspects could lead to inaccurate trajectory tracking of the quadcopter system and, finally, result in an unstable control system. To handle these challenges, numerous robust control methods have been designed to control the nonlinear dynamical systems including the quadcopter system, for instance, the sliding mode control (SMC) [2]–[4], feedback linearization [5], [6], adaptive SMC control [7]–[9], second-order sliding mode control [10], super-twisting sliding mode control [11], high-order sliding mode control [12], and robust backstepping control [13], [14].

The SMC is well-known for its robustness against unknown dynamics and external disturbances [7], [15], [16].

The associate editor coordinating the review of this manuscript and approving it for publication was Shihong Ding.

Typically, SMC consists of two control terms, the equivalent and the switching controls. The equivalent control is calculated based on the Lyapunov theorem to cancel the nonlinear dynamics, while the switching control absorbs the effect of unknown uncertainty and unmodeled dynamics. The main drawback of the SMC is the chattering phenomena [17], [18]. The chattering is proportionally increased by the increment of the SMC switching gain value. However, for achieving robust stability the values of the switching gains must be larger than the upper bound of the uncertainty and unmodeled dynamics. Practically, the upper bound of the uncertainty and unmodeled terms are usually unknown for physical systems. In such situations, the values of the switching gains should be large enough to cover a wide range of uncertainties, unmodeled dynamics, and disturbances. As a result of the selection of high switching gains, the chattering is induced at high amplitudes and frequencies, in which the state variables oscillate around the sliding manifold [19]. The chattering causes critical problems in the physical systems, for example, the vibration in the quadcopter's mechanical body and the generation of heat in the onboard computer's electronics kits, which lead to increase power consumption.

The challenge is to benefit the SMC control in terms of its robustness against the unknown upper bound of the uncertainties and unmodeled dynamics while attenuating the chattering to an acceptable limit. Such a challenge is motivating the researchers to reinforce the SMC control to handle the chattering drawback in addition to achieve robust trajectory tracking. For instance, the boundary layer [20], higher-order control [21], and fuzzy gain scheduling [22]–[25] are reported in the literature to reduce the chattering influence. These techniques still depend on the knowledge of the limits of the upper bound of the parameter's uncertainties.

An adaptive sliding mode control (ASMC) has been developed in which the switching gains are adaptively tuned according to changes in the parameter's uncertainties [26], [27]. A robust trajectory tracking has been achieved; however the proposed ASMC does not consider the chattering attenuation. An adaptive law is proposed in [28] whereas a fast adaptation and significant chattering attenuation have been attained.

In this paper, the quadcopter dynamic has been divided into two parts, the attitude dynamics, and the position dynamics subsystems. An improved adaptive sliding mode (IASMC) control strategy has been developed to control the quadcopter's attitude, while an interval type-2 fuzzy PID (IT2-FPID) controller has been adopted to control the quadcopter's position. The aim of this research is to benefit of the SMC control advantages, the robustness against uncertainties, meanwhile overcome the chattering phenomenon associated with conventional SMC.

The main contributions of this research are as following:

- Estimating SMC switching gains based on an improved adaptive formula that offers a fast adaptation speed against the changes in the model uncertainties, meanwhile attenuating the chattering impact.

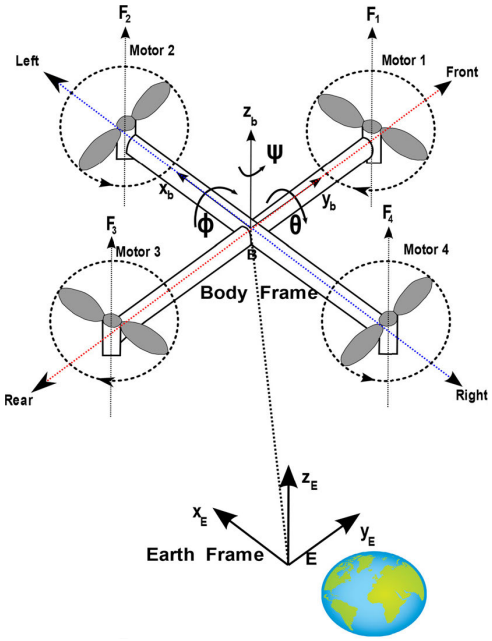

FIGURE 1. Quadcopter UAV configuration and the rotors numbering [31].

- Presenting an adaptive control law based on the Lyapunov approach to estimate the equivalent control term, that handles a nontrivial part of uncertainties and relieve the burden on the switching control term. Unlike [28], where only the switching control term carry the burden of uncertainties.
- Replacing the switching function (sign(s)) by smooth function (error function) which contributes further to the chattering attenuation.
- Designing an IT2-FPID as an outer loop controller, that can adapt to the variations in uncertainties while generating accurate desired angles to the inner loop controller for an arbitrary desired path.

The rest of the manuscript is organized in the following outline. In Section II, the quadcopter kinematic and dynamic equations, along with the description, have been briefly presented. Section III is dedicated to the proposed IASMC and IT2-FPID controllers to control the quadcopter's attitude and position, respectively. In section IV, proposed controllers have been evaluated by using simulations and the results have been presented and discussed. Section V concludes the paper with a summary and future work.

II. QUADCOPTER DYNAMICS MODEL

A. QUADCOPTER SYSTEM DESCRIPTION

The quadcopter UAV consists of four rotors to generate (F_1, F_2, F_3, F_4) mounted in a intersect configuration [29], [30], as shown in Figure 1 with the symmetric shape.

The quadcopter moves in space in 6-DOFs (the attitude and position). As we can see, Figure 2 and Table 1 map all of the possible movements in the space: take-off, landing, right, left, forward, backward, clockwise, and counterclockwise directions. The arrow thickness in Figure 2 is proportional to

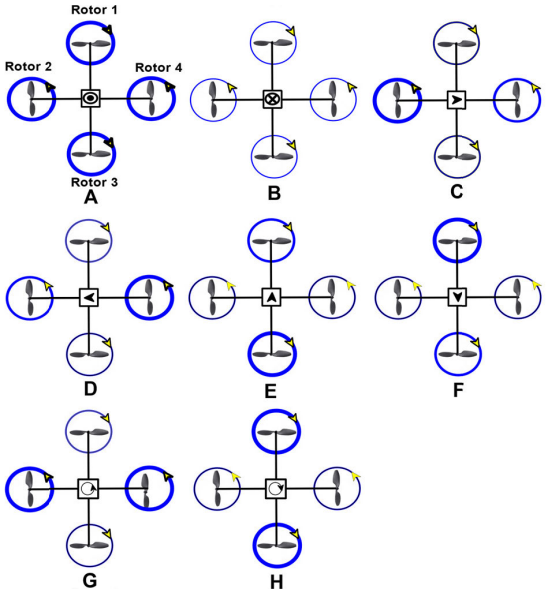

FIGURE 2. Quadcopter UAV possible motions.

TABLE 1. The quadcopter UAV possible movements.

Motors & Movements	Rotor 1	Rotor 2	Rotor 3	Rotor 4
Take-off				
Landing				
Right				
Left				
Forward				
Backward				
Clockwise				
Anti-Clockwise				

the rotor speed. • indicates the up direction, and ⊗ indicates the down direction.

B. QUADCOPTER KINEMATICS MODELING

The quadcopter kinematics equations can be represented in two frames: the earth fixed frame (E-frame) or the reference frame and denoted by $\boldsymbol{E}$=(x_e, y_e, z_e), and the body fixed (B-frame) $\boldsymbol{B}$=(x_b, y_b, z_b). The quadcopter's coordinates can be written as:

$$\boldsymbol{q} = [\boldsymbol{\xi}, \boldsymbol{\eta}]^T \tag{1}$$

where,

$$\boldsymbol{\xi} = [x, y, z]^T \tag{2}$$

and,

$$\boldsymbol{\eta} = [\phi, \theta, \psi]^T \tag{3}$$

The kinematic equations can be written as the following:

$$\dot{\boldsymbol{\xi}} = \boldsymbol{RV} \tag{4}$$

where V represents the linear velocity in the B-frame, while ξ is the linear velocity in the E-frame, and R is the rotation matrix (5), as shown at the bottom of the page. The quadcopter rotational motion is obtained as the following:

$$\dot{\boldsymbol{\eta}} = \boldsymbol{T\omega} \tag{6}$$

where $\boldsymbol{\omega}$ represents the angular velocity in the B-frame, while $\dot{\boldsymbol{\eta}}$ represents the angular velocity in the E-frame. **T** is the transfer matrix [32]:

$$\boldsymbol{T} = \begin{bmatrix} 1 & \sin\phi\tan\theta & \cos\phi\tan\theta \\ 0 & \cos\phi & -\sin\phi \\ 0 & \dfrac{\sin\phi}{\cos\theta} & \dfrac{\cos\phi}{\cos\theta} \end{bmatrix} \tag{7}$$

C. QUADCOPTER DYNAMIC MODEL

The quadcopter UAV dynamics in 6-DOF are given as follows:

$$\begin{aligned}
\ddot{x} &= (\cos\phi\sin\theta\cos\psi + \sin\phi\sin\psi)\frac{u_1}{m} \\
\ddot{y} &= (\cos\phi\sin\theta\cos\psi - \sin\phi\sin\psi)\frac{u_1}{m} \\
\ddot{z} &= -g + (\cos\phi\cos\theta)\frac{u_1}{m} \\
\ddot{\phi} &= a_1\dot{\theta}\dot{\psi} + a_2\dot{\theta}\Omega_d + \frac{1}{I_x}u_2 \\
\ddot{\theta} &= a_3\dot{\phi}\dot{\psi} + a_4\dot{\phi}\Omega_d + \frac{1}{I_y}u_3 \\
\ddot{\psi} &= a_5\dot{\phi}\dot{\theta} + \frac{1}{I_z}u_4
\end{aligned} \tag{8}$$

where

$$a_1 = \frac{I_y - I_z}{I_x}, a_2 = \frac{J_r}{I_x}, a_3 = \frac{I_z - I_x}{I_y}, a_4 = \frac{J_r}{I_y}, \quad and \quad a_5 = \frac{I_x - I_y}{I_z}$$

and, (u_1, u_2, u_3, u_4) are the control inputs given as follows:

$$\begin{aligned}
u_1 &= b(\Omega_1^2 + \Omega_2^2 + \Omega_3^2 + \Omega_4^2) \\
u_2 &= b(\Omega_4^2 - \Omega_2^2) \\
u_3 &= b(\Omega_3^2 - \Omega_1^2) \\
u_4 &= d(\Omega_4^2 + \Omega_2^2 - \Omega_3^2 - \Omega_1^2)
\end{aligned} \tag{9}$$

and, Ω_d is expressed as follows:

$$\Omega_d = -\Omega_1 + \Omega_2 - \Omega_3 + \Omega_4 \tag{10}$$

$$\boldsymbol{R} = \begin{bmatrix} \cos\theta\cos\psi & \sin\phi\sin\theta\cos\psi - \cos\phi\cos\psi & \sin\phi\sin\theta\cos\psi + \cos\phi\sin\psi \\ \cos\theta\sin\psi & \sin\phi\sin\theta\sin\psi + \cos\phi\cos\psi & \cos\phi\sin\theta\sin\psi - \sin\phi\cos\psi \\ -\sin\theta & \sin\phi\cos\theta & \cos\phi\cos\theta \end{bmatrix} \tag{5}$$

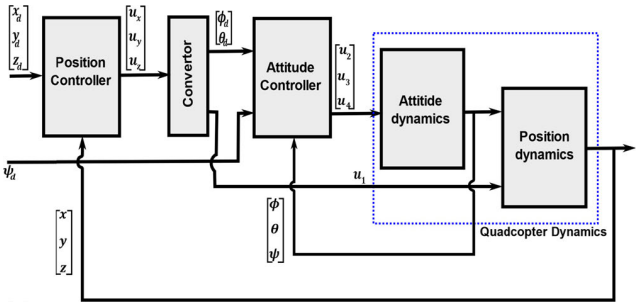

FIGURE 3. Overall quadcopter control system block diagram [31].

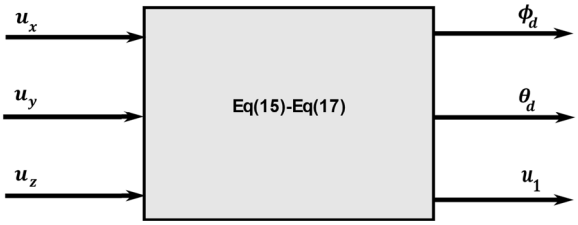

FIGURE 4. Virtual control inputs and outputs [33].

III. CONTROL DESIGN

As shown in Figure 3, the proposed IASMC is designed to stabilize the quadcopter's attitude, and the interval type-2 fuzzy PID (IT2-FPID) is implemented to control the quadcopter's position and provide the desired values of the attitude to the IASMC controller.

A. TYPE-2 FUZZY PID OUTER LOOP CONTROLLER DESIGN

The quadcopter dynamic equations in (9) are underactuated dynamics due to the outputs $[x, y, z, \phi, \theta, \psi]^T$ which are controlled by $[u_1, u_2, u_3, u_4]^T$ only. The type-2 fuzzy PID is designed to control the quadcopter's position as in [33], [34]. The quadcopter's position is an underactuated subsystem as expressed below:

$$\begin{aligned}\ddot{x} &= (\cos\phi \sin\theta \cos\psi + \sin\phi \sin\psi)\frac{u_1}{m}\\ \ddot{y} &= (\cos\phi \sin\theta \cos\psi - \sin\phi \sin\psi)\frac{u_1}{m}\\ \ddot{z} &= -g + (\cos\phi \cos\theta)\frac{u_1}{m}\end{aligned} \tag{11}$$

The above equation (12) can be written in the follows:

$$u = \begin{bmatrix} u_x \\ u_y \\ u_z \end{bmatrix} = \begin{bmatrix} \cos\phi \sin\theta \cos\psi + \sin\phi \sin\psi \\ \cos\phi \sin\theta \cos\psi - \sin\phi \sin\psi \\ \cos\phi \cos\theta \end{bmatrix} \frac{u_1}{m} - \begin{bmatrix} 0 \\ 0 \\ g \end{bmatrix} \tag{12}$$

where $u = [\ddot{x}, \ddot{y}, \ddot{z}]^T$.

The virtual controls are used to control the quadcopter's positions x, y, and z axis via (u_1, ϕ_d and θ_d). As illustrated in Figure 3, the outer loop controller receives the desired values of the position (x_d, y_d, z_d) and actual (x, y, z) trajectory to generate the virtual controls (u_x, u_y, u_z). While the convertor receives the virtual controls inputs and provides the lift force (u_1), desired rolling (ϕ_d), and desired pitching (θ_d) angles as shown in Figure 4.

Equations (12), and (13), can be rewritten as follows:

$$\begin{aligned}u_x &= \frac{u_1}{m}(\cos\phi \sin\theta \cos\psi + \sin\phi \sin\psi)\\ u_y &= \frac{u_1}{m}(\cos\phi \sin\theta \cos\psi - \sin\phi \sin\psi)\\ u_z &= \frac{u_1}{m}(\cos\phi \cos\theta) - g\end{aligned} \tag{13}$$

The control aim is to design an outer loop IT2-FPID controller to stabilize the error's position dynamics (15). Where the desired position is represented by (x_d, y_d, z_d), and the measured position is given by (x, y, z).

$$\begin{aligned}e_x &= x - x_d\\ e_y &= y - y_d\\ e_z &= z - z_d\end{aligned} \tag{14}$$

With some mathematical manipulations of (14), leads to:

$$u_1 = \sqrt{u_x^2 + u_y^2 + (u_z + g)^2} \tag{15}$$

and,

$$\phi_d = \sin^{-1}\left(\frac{u_x \sin\psi_d - u_y \cos\psi_d}{u_1}\right) \tag{16}$$

$$\theta_d = \tan^{-1}\left(\frac{u_x \sin\psi_d + u_y \cos\psi_d}{u_z + g}\right) \tag{17}$$

The fuzzy logic controller (FLCs) performs better, especially if the controlled plant shows a nonlinear behavior. FLCs are nonlinear controllers that receive the knowledge about the plant in the form of linguistic IF-THEN rules and then renovate this knowledge into a mathematical formulation that has been established as being very effective in numerous applications. Other model-based nonlinear controllers require the mathematical model to be represented in a format that satisfies certain conditions. In contrast, FLCs are independent of the mathematical system model, which can be useful in controlling complex systems with proper experience about their operation [35], [36].

The type-1 fuzzy logic system (FLS) incorporates four elements: fuzzifier, rules base, inference engine, and a defuzzifier. The well-designed type-1 FLC effectively handles the system nonlinearity; however, the controller performance may degrade under the presence of uncertainty in the manipulated system due to linguistic uncertainty where linguistic expression can be interpreted differently by different individuals. The type-2 fuzzy set theory addresses this issue by using uncertain membership functions with a lower and an upper bound. The area between these bounds is defined as the footprint of uncertainty (FOU), which has led to the advent of a new class of fuzzy systems called Type-2 FLS (T2-FLS). As illustrated in Figure 5 this has a similar architecture with the last element replaced by an output processor, which consists of a two-stage type reduction from type-2 to type-1 and the defuzzification. General Type-2 FLS are costly in terms of computation due to the type reduction process compare to the interval type-2 FLS (IT2-FLS) [37], [38].

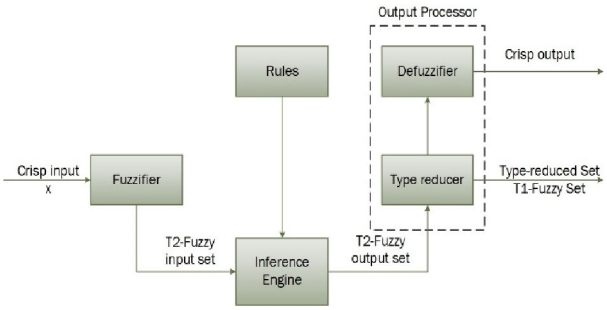

FIGURE 5. The general architecture of T2-FLS.

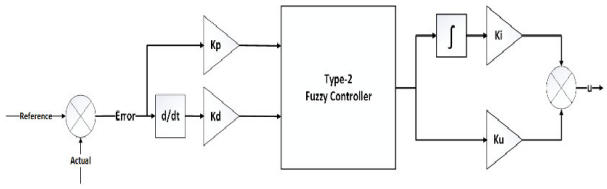

FIGURE 6. Interval Type-2 Fuzzy PID controller block diagram.

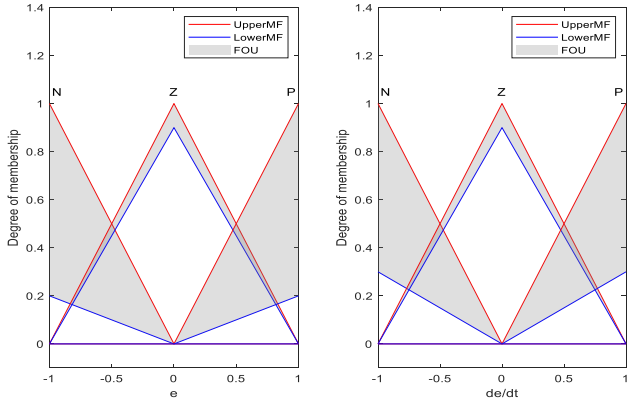

FIGURE 7. IT-2 FLC inputs membership functions.

Using the centroid method the defuzzified output is given by [39]:

$$u = \frac{y_l + y_r}{2} \tag{18}$$

where,

$$y_l = \frac{\sum_{i=1}^{L} x_i \mu_{umf}(x_i) + \sum_{i=L+1}^{N} x_i \mu_{lmf}(x_i)}{\sum_{i=1}^{L} \mu_{umf}(x_i) + \sum_{i=L+1}^{N} \mu_{lmf}(x_i)} \tag{19}$$

and

$$y_r = \frac{\sum_{i=1}^{R} x_i \mu_{lmf}(x_i) + \sum_{i=R+1}^{N} x_i \mu_{umf}(x_i)}{\sum_{i=1}^{R} \mu_{lmf}(x_i) + \sum_{i=R+1}^{N} \mu_{umf}(x_i)} \tag{20}$$

N denotes the number of samples whereas μ_{lmf} and μ_{umf} represent the lower and upper membership functions, respectively. x_i represents the output of the i^{th} sample. R and L are switch points that can be estimated by Karnik-Mendel algorithm.

The input membership functions of the proposed (IT2-FPID) are demonstrated in Figure 7, where each input composes three sets, namely negative (N), zero (Z), and positive (P). Figure 8 illustrates the rules surface.

Table 2 demonstrates the FLC's rule. A uniform set is adopted for both FLC's inputs and output, where the input

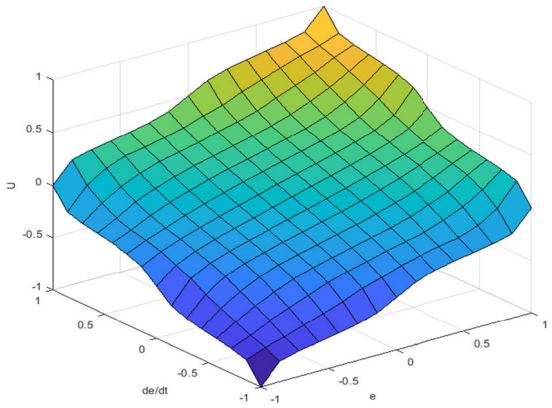

FIGURE 8. IT-2 FLC rules surface.

TABLE 2. Fuzzy rules.

	N	Z	P
N	N	N	Z
Z	B	M	P
P	M	Z	M
	Z	P	P
		M	B

is defined as {N, Z, P}.The output set has been selected as {NB, NM, Z, PM, PB} where NB, NM, PB, and PM denote negative big, negative medium, positive medium, and positive big, respectively.

B. THE IMPROVED ADAPTIVE SLIDING MODE CONTROL DESIGN

The scope of the IASMC controller design will cover the quadcopter's attitude subsystem dynamics equations only, as follows:

$$\begin{aligned}
\ddot{\phi} &= a_1\dot{\theta}\dot{\psi} + a_2\dot{\theta}\Omega_d + \frac{1}{I_x}u_2 + \mu_\phi \\
\ddot{\theta} &= a_3\dot{\phi}\dot{\psi} + a_4\dot{\phi}\Omega_d + \frac{1}{I_y}u_3 + \mu_\theta \\
\ddot{\psi} &= a_5\dot{\phi}\dot{\theta} + \frac{1}{I_z}u_4 + \mu_\psi
\end{aligned} \tag{21}$$

where,

$$a_1 = \frac{I_y - I_z}{I_x}, a_2 = \frac{J_r}{I_x}, a_3 = \frac{I_z - I_x}{I_y}, a_4 = \frac{J_r}{I_y}, \text{ and } a_5 = \frac{I_x - I_y}{I_z}$$

and $\mu_\phi, \mu_\theta, \mu_\psi$ are the lumped uncertainties for ϕ, θ, ψ dynamics, respectively.

The control objective is to propose an improved ASMC controller to stabilize the error's attitude dynamics. where $(\phi_d, \theta_d, \psi_d)$ is the desired attitude, and (ϕ, θ, ψ) is the actual attitude. The error's attitude dynamic is given by:

$$\begin{aligned}
e_\phi &= \phi - \phi_d \\
e_\theta &= \theta - \theta_d \\
e_\psi &= \psi - \psi_d
\end{aligned} \tag{22}$$

The proposed IASMC controller has been designed based on the following steps:

Step 1: is to determine the error dynamics as in (23).

Step 2: is to write the sliding surface as follows, [3]:

$$s = \left(\frac{d}{dt} + k_x\right)^{n-1} e \tag{23}$$

Thus, the sliding surfaces for attitude angles are

$$\begin{aligned} s_\phi &= \dot{e}_\phi + k_\phi e_\phi \\ s_\theta &= \dot{e}_\theta + k_\theta e_\theta \\ s_\psi &= \dot{e}_\psi + k_\psi e_\psi \end{aligned} \tag{24}$$

where, s_ϕ, s_θ and s_ψ defined the sliding surfaces for roll, pitch, and yaw, respectively. While k_ϕ, k_θ and k_ψ are positive constants.

Step 3: is to use the sliding mode condition as the following,

$$\dot{s} = -k_1 sgn(s) - k_2 s \tag{25}$$

Substitute (25) into (26), yields to,

$$\begin{aligned} \ddot{e}_\phi + k_\phi \dot{e}_\phi &= -k_{1_\phi} sgn(s_\phi) - k_{2_\phi} s_\phi \\ \ddot{e}_\theta + k_\theta \dot{e}_\theta &= -k_{1_\theta} sgn(s_\theta) - k_{2_\theta} s_\theta \\ \ddot{e}_\psi + k_\psi \dot{e}_\psi &= -k_{1_\psi} sgn(s_\psi) - k_{2_\psi} s_\psi \end{aligned} \tag{26}$$

Substitute (22) and (23) into (27), yields to,

$$\begin{aligned} &a_1 \dot{\theta}\dot{\psi} + a_2 \dot{\theta}\Omega_d + \frac{1}{I_x} u_2 + \mu_\phi - \ddot{\phi}_d + k_\phi \dot{e}_\phi \\ &\quad = -k_{1_\phi} sgn(s_\phi) - k_{2_\phi} s_\phi \\ &a_3 \dot{\phi}\dot{\psi} + a_4 \dot{\phi}\Omega_d + \frac{1}{I_y} u_3 + \mu_\theta - \ddot{\theta}_d + k_\theta \dot{e}_\theta \\ &\quad = -k_{1_\theta} sgn(s_\theta) - k_{2_\theta} s_\theta \\ &a_5 \dot{\phi}\dot{\theta} + \frac{1}{I_z} u_4 + \mu_\psi - \ddot{\psi}_d + k_\psi \dot{e}_\psi \\ &\quad = -k_{1_\psi} sgn(s_\psi) - k_{2_\psi} s_\psi \end{aligned} \tag{27}$$

where $k_{1_\phi}, k_{1_\theta}, k_{1_\psi} > 0$ and $k_{2_\phi}, k_{2_\theta}, k_{2_\psi} > 0$ are the SMC control gains.

Step 4: is to cancel the nonlinear terms and uncertainty in the parameters in (28), the control input u_2, u_3, u_4 are selected as follows:

$$\begin{aligned} u_2 &= I_x \left(\ddot{\phi}_d - a_1 \dot{\theta}\dot{\psi} - a_2 \dot{\theta}\Omega_d - k_\phi \dot{e}_\phi + \mu_\phi + U_1\right) \\ u_3 &= I_y \left(\ddot{\theta}_d - a_3 \dot{\phi}\dot{\psi} - a_4 \dot{\phi}\Omega_d - k_\theta \dot{e}_\theta + \mu_\theta + U_2\right) \\ u_4 &= I_z \left(\ddot{\psi}_d - a_5 \dot{\phi}\dot{\theta} - k_\psi \dot{e}_\psi + \mu_\psi + U_3\right) \end{aligned} \tag{28}$$

Substitute (29) into (28), along with (27) leads to:

$$\begin{aligned} \dot{s}_\phi &= U_1 + \zeta_\phi \\ \dot{s}_\theta &= U_2 + \zeta_\theta \\ \dot{s}_\psi &= U_3 + \zeta_\psi \end{aligned} \tag{29}$$

where,

$$\begin{aligned} \zeta_\phi &= I_x \mu_\phi \\ \zeta_\theta &= I_y \mu_\theta \\ \zeta_\psi &= I_z \mu_\psi \end{aligned} \tag{30}$$

Step 5: is to obtain the estimated uncertainty $\zeta_\phi, \zeta_\theta, \zeta_\psi$ based on the following selected Lyapunov functions:

$$\begin{aligned} V_\phi &= \frac{1}{2} s_\phi^2 + \frac{1}{2} \tilde{\zeta}_\phi \gamma_\phi \tilde{\zeta}_\phi \\ V_\theta &= \frac{1}{2} s_\theta^2 + \frac{1}{2} \tilde{\zeta}_\theta \gamma_\theta \tilde{\zeta}_\theta \\ V_\psi &= \frac{1}{2} s_\psi^2 + \frac{1}{2} \tilde{\zeta}_\psi \gamma_\psi \tilde{\zeta}_\psi \end{aligned} \tag{31}$$

where, $\tilde{\zeta}_\phi, \tilde{\zeta}_\theta, \tilde{\zeta}_\psi$ are the error between the actual uncertainty and the estimated uncertainty $\tilde{\zeta}_\phi = \zeta_\phi - \hat{\zeta}_\phi$, $\tilde{\zeta}_\theta = \zeta_\theta - \hat{\zeta}_\theta$, and $\tilde{\zeta}_\psi = \zeta_\psi - \hat{\zeta}_\psi$, while, γ_ϕ, γ_θ, and γ_ψ are positive constants. Thus, by differentiating both sides of the equation (32) yields to:

$$\begin{aligned} \dot{V}_\phi &= s_\phi \dot{s}_\phi + \dot{\tilde{\zeta}}_\phi \gamma_\phi \tilde{\zeta}_\phi \\ \dot{V}_\theta &= s_\theta \dot{s}_\theta + \dot{\tilde{\zeta}}_\theta \gamma_\theta \tilde{\zeta}_\theta \\ \dot{V}_\psi &= s_\psi \dot{s}_\psi + \dot{\tilde{\zeta}}_\psi \gamma_\psi \tilde{\zeta}_\psi \end{aligned} \tag{32}$$

According to (33) the adaption laws are set as follows

$$\dot{\hat{\zeta}}_\phi = \frac{1}{\gamma_\phi} s_\phi \dot{\hat{\zeta}}_\theta = \frac{1}{\gamma_\theta} s_\theta \dot{\hat{\zeta}}_\psi = \frac{1}{\gamma_\psi} s_\psi \tag{33}$$

Thus, from equation (33), the control inputs will be as follows

$$\begin{aligned} U_1 &= -\hat{\zeta}_\phi - k_{1_\phi} sgn(s_\phi) - k_{2_\phi} s_\phi \\ U_2 &= -\hat{\zeta}_\theta - k_{1_\theta} sgn(s_\theta) - k_{2_\theta} s_\theta \\ U_3 &= -\hat{\zeta}_\psi - k_{1_\psi} sgn(s_\psi) - k_{2_\psi} s_\psi \end{aligned} \tag{34}$$

Step 6: is well known: to ensure the control system robustness against the unknown upper bound on the modeling uncertainties and disturbances, the control gains, k_{1_ϕ}, k_{1_θ}, and k_{1_ψ} in (35) must be as large as possible to cover a wide-range of expected upper bounds on the unknown uncertain terms. However, the price of the large control gains selection leads to the chattering phenomenon, which is unwanted and causes many problems, for instance, the vibrations in the mechanical parts. Therefore, to reduce the chattering impact to some degree, the control gains k_{1_ϕ}, k_{1_θ}, and k_{1_ψ} can be estimated as in (33) as follows [26]:

$$\begin{aligned} \dot{\hat{k}}_{1_\phi} &= \beta_\phi \left| s_\phi \right| \\ \dot{\hat{k}}_{1_\theta} &= \beta_\theta \left| s_\theta \right| \\ \dot{\hat{k}}_{1_\psi} &= \beta_\psi \left| s_\psi \right| \end{aligned} \tag{35}$$

where, β_ϕ, β_θ, and β_ψ are positive constants. However, in this approach, the chattering still happens due to the slow adaptation speed around the sliding surface, which is caused by the slow variation on the switching gains. While, on the other side, a rapid change in the uncertainties and disturbances of the parameter may occur. This mismatching between the adaptation speed and the changes in parameter uncertainties leads to a dramatic increment in the switching gains to ensure the control system stability and trajectory tracking robustness, and at this point, the chattering occurs.

Step 7: Another factor that has a significant impact and which induces the chattering phenomenon is the switching function (sign(s)) in the control law (35). One technique that

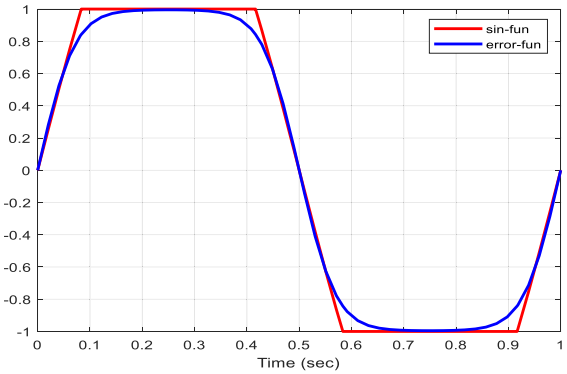

FIGURE 9. The switching functions (sign and error functions).

TABLE 3. The quadcopter's Parameters.

Name	Parameter	Value	Unit
Mass	m	65×10^{-2}	kg
inertia on x-axis	I_x	75×10^{-4}	kgm^2
inertia on y-axis	I_y	75×10^{-4}	kgm^2
inertia on z-axis	I_z	13×10^{-3}	kgm^2
thrust coefficient	b	313×10^{-6}	Ns^2
drag coefficient	d	7.5×10^{-7}	Nms^2
rotor inertia	J_r	6×10^{-5}	kgm^2
arm length	l	23×10^{-2}	m

participates in the chattering reduction is to approximate the sign(s) with the error function (erf(s)). Therefore the switching function in (35) will be changed by the error function (erf(s)) in (37), which provides smooth changes in the control law as depicted in Figure 9.

$$efr\ (s) = \frac{2}{\sqrt{\pi}} \int_0^s e^{-t^2} dt \tag{36}$$

and has properties:

$$erf\ (+\infty) = 1, erf\ (-\infty) = -1$$

Step 8: Further improvement has been proposed in the control laws (35) in which the switching gains are designed in such a way (38) to balance between the speed of changes in the parameter uncertainties and the switching gain adaptation speed (gains variation speed). As it can be observed there are three parameters in (38) that govern the adaptation speed in the proposed switching gains, φ_i, α_i and $\delta_i\ (t)$.

$$\dot{\hat{k}}_i = \begin{cases} \varphi_i \left\{ \alpha_i^{-1} \cdot |s_i\ (t)| \right\}^{-\delta_i(t)} \cdot \delta_i\ (t) & if\ \hat{k}_i > 0 \\ \varphi_i \cdot \alpha_i^{-1} \cdot |s_i\ (t)| & if\ \hat{k}_i = 0 \end{cases} \tag{37}$$

However, to control the rate of change of the control gains $\hat{k}_i$ based on the chattering reduction demand, the parameter φ_i can be tuned as follows:

$$\delta_i\ (t) = \text{erf}\ \|s_i\ (t)\|_\infty - \epsilon_i) \tag{38}$$

$$\varphi_i = \begin{cases} \varphi_{i_{up}} & if\ \delta_i\ (t) > 0 \\ \varphi_{i_{down}} & if\ \delta_i\ (t) \leq 0 \end{cases} \tag{39}$$

where, $\varphi_{i_{up}}$ controls the increment rate and $\varphi_{i_{down}}$ controls the decrement rate.

TABLE 4. (IT2-FPID) controller gains.

Symbols	x	y	z
k_P	5	5	10
k_I	1	1	5
k_D	4	4	3
k_u	10	10	10

TABLE 5. ASMC controller gains.

Symbols	ϕ	θ	ψ
k_2	0.01	0.01	0.01
γ	5	5	5
β	0.1	0.05	0.1

TABLE 6. The IASMC controller gains.

Symbols	ϕ	θ	ψ
k_2	0.01	0.01	0.01
γ	5	5	5
β	0.1	0.05	0.1
ε	0.005	0.01	0.02
φ_{up}	0.6	0.8	0.4
φ_{down}	5	8	2
α	50	50	1

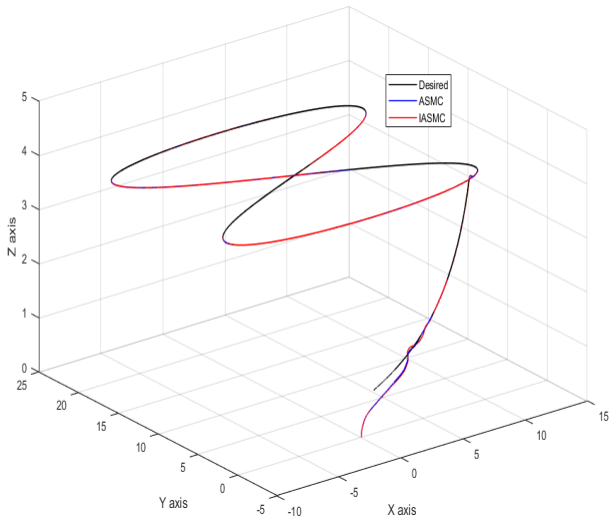

FIGURE 10. Comparison of the ASMC and IASMC performance.

IV. SIMULATION MODEL

The quadcopter model has been simulated using Matlab/Simulink environment; the quadcopter's parameters used in this simulation are taken from [40], and listed in Table 3. While the controller's parameters are presented in Table 4, Table 5, and Table 6 for (IT2-FPID), ASMC, and IASMC controllers, respectively.

V. SIMULATION RESULTS AND DISCUSSION

In this section, the simulation is conducted using SIMULINK to test the performance of the proposed controller considering two scenarios: firstly, the performance without model

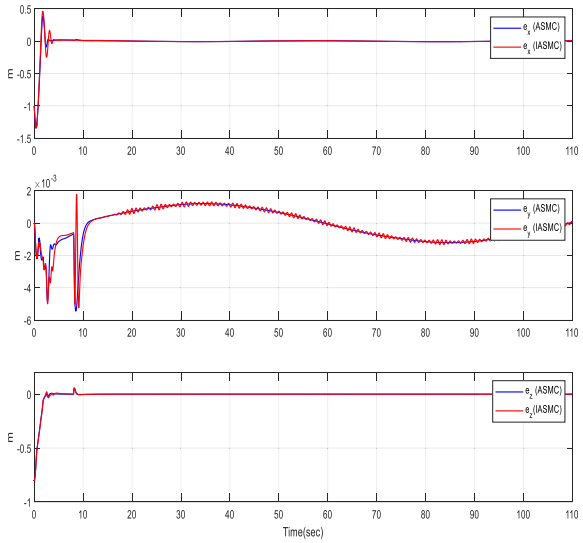

FIGURE 11. The error in the quadcopter positions.

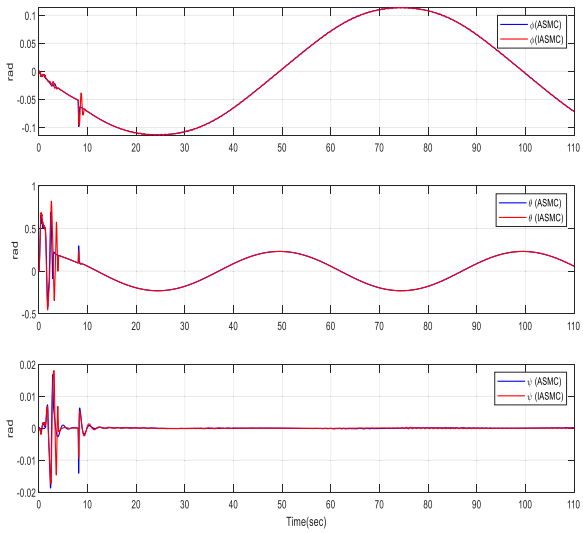

FIGURE 12. The quadcopter attitude trajectory tracking.

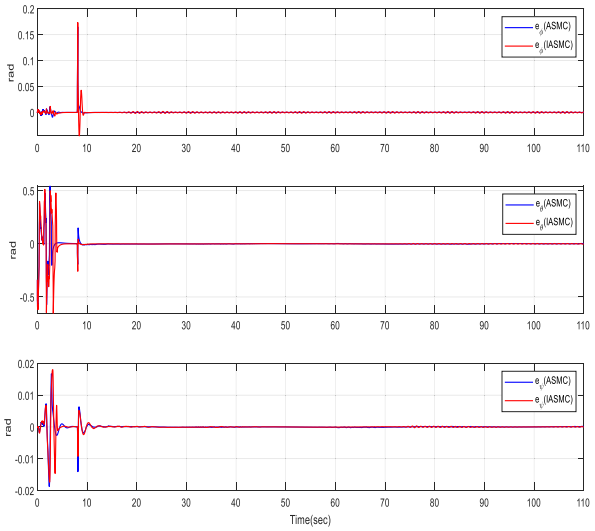

FIGURE 13. The error in the quadcopter attitude.

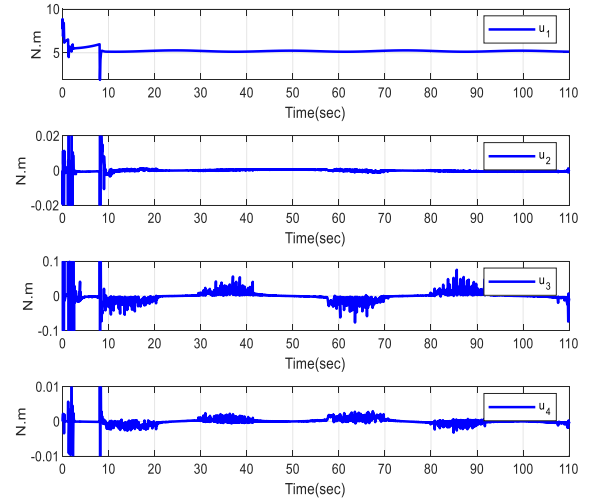

FIGURE 14. The control signals of the quadcopter with a constant switching gain.

uncertainty and then the performance under the presence of uncertainty. The uncertainty is considered in the quadcopter mass, owing to it is a crucial impact on the system's dynamic. Moreover, the proposed controller has been compared with ASMC in terms of chattering reduction and trajectory tracking error. The simulation has been conducted on two levels. Primarily, ASMC is implemented based on the control law in (35) where the switching gain is calculated adaptively as in (36). Then for further enhancement of the chattering attenuation, the switching gains are recalculated based on (38), and the sign function is approximated by the error function (37) to get a smooth switching as depicted in Figure 9.

A. CONTROL SYSTEM PERFORMANCE UNDER IDEAL CONDITIONS

In this scenario, the system is simulated, assuming the ideal case in which the exact parameters' values of the quadcopter system are considered. Figure 10 demonstrates the tracking performance of ASMC and IASMC, considering a 3D 8-shape as the desired trajectory. Figure 11 shows the quadcopter position error in the x, y, and z axes. While Figures 12 and 13 depict the quadcopter attitude (ϕ, θ, ψ) tracking and attitude error, respectively. Based on the position and attitude tracking errors, both controllers provide excellent performance. However, in terms of the chattering attenuation in the quadcopter control signals, the proposed IASMC, as presented in Figure 16, outperforms the ASMC with a constant switching gain and an adaptive switching gain, as shown in Figures 14 and 15, respectively. This significant reduction in chattering in the case of IASMC is due to its switching mechanism. The gains are slightly higher when the error is high and smaller when the system's trajectories are very close to the sliding manifold. In contrast, the ASMC does not exhibit any reduction in switching gains, which are either increasing or at a constant level, as displayed in Figure 17.

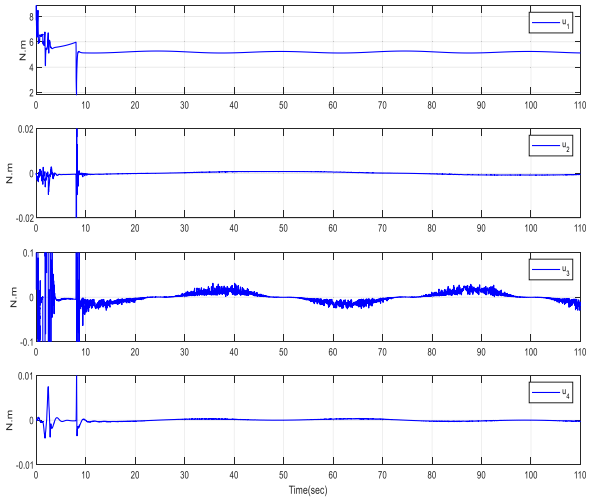

FIGURE 15. The control signals of the quadcopter with the ASMC controller.

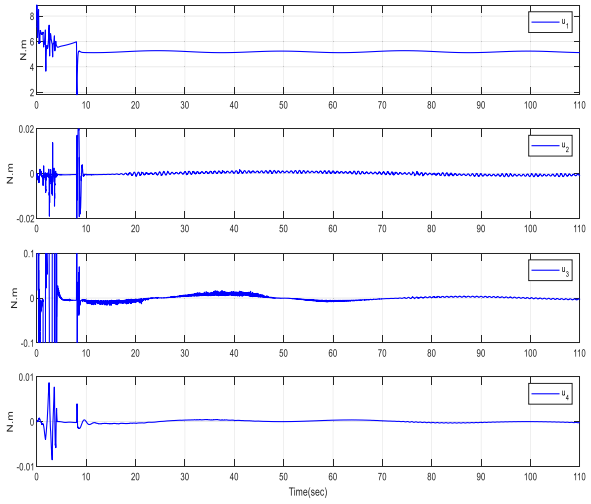

FIGURE 16. The control signals of the quadcopter with the IASMC controller.

B. THE CONTROL SYSTEM PERFORMANCE UNDER UNCERTAINTY

In this scenario, the system is simulated in the presence of uncertainty in the quadcopter's mass and assumed to be as presented in Figure 18. This may occur in real-world quadcopter applications including but not limited to payload-carrying, crop spraying and product delivery. Figure 19 visualizes the 3-D 8-shape trajectory tracking for both ASMC and IASMC. Figure 20 presents the quadcopter position error. Whereas Figures 21 and 22 illustrate the quadcopter attitude (ϕ, θ, ψ) tracking and its error, respectively. As stated in the previous scenario, both controllers almost present similar performance in terms of position and attitude tracking errors.

Still, in terms of the chattering attenuation in the quadcopter control signals, the proposed IASMC, as presented in Figure 25, outperforms the ASMC with a constant switching gain and an adaptive switching gain, as shown in Figures 23 and 24. The switching gains for ASMC and IASMC are illustrated in Figure 26, wherein the ASMC

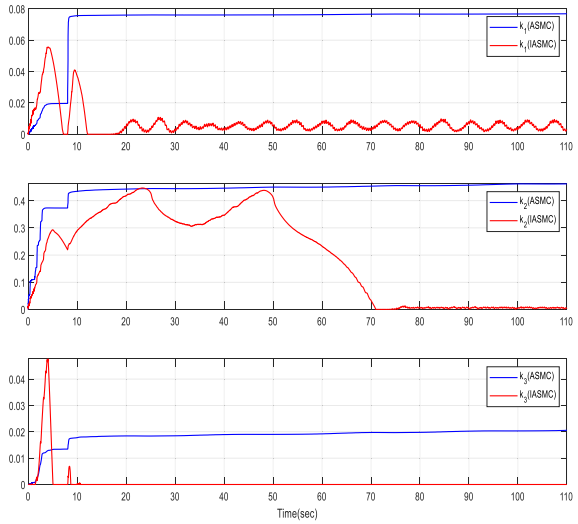

FIGURE 17. The switching gains for ASMC & IASMC.

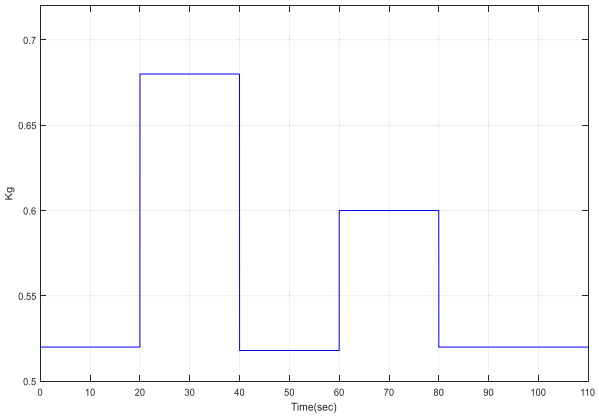

FIGURE 18. Injected Mass Uncertainty of the Quadcopter.

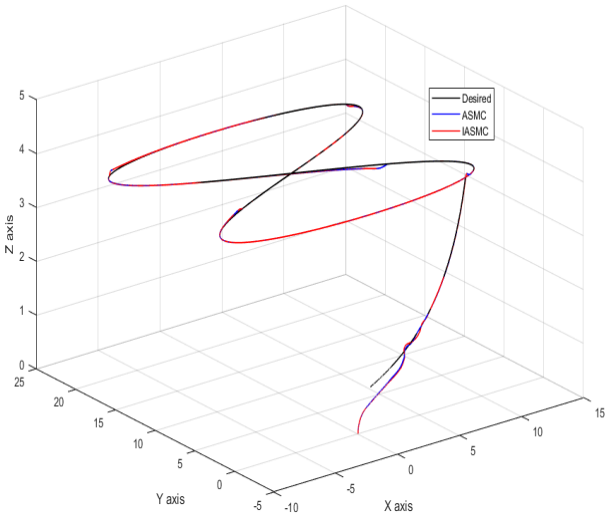

FIGURE 19. 8-Shape trajectory tracking.

switching gains rapidly increase to cover a wide-range of the unknown and unbounded uncertainty; as a result, the chattering is increased. While in the IASMC, the switching gains

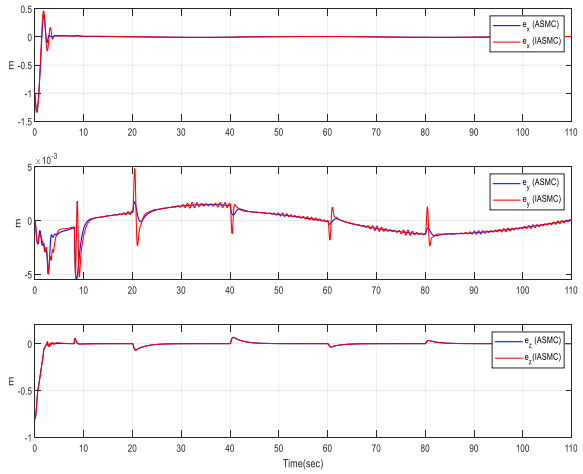

FIGURE 20. The error in the quadcopter positions.

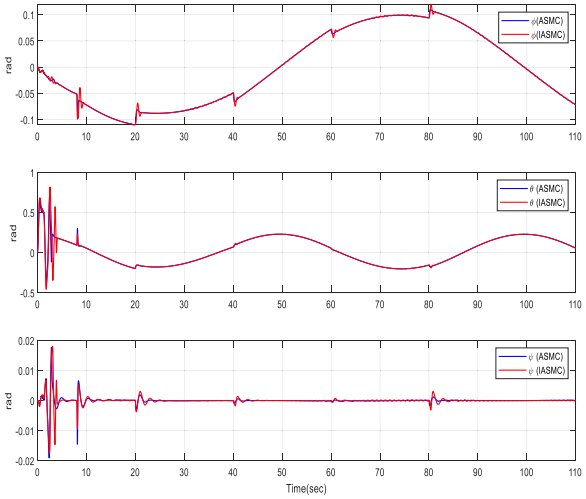

FIGURE 21. The quadcopter attitude trajectory tracking.

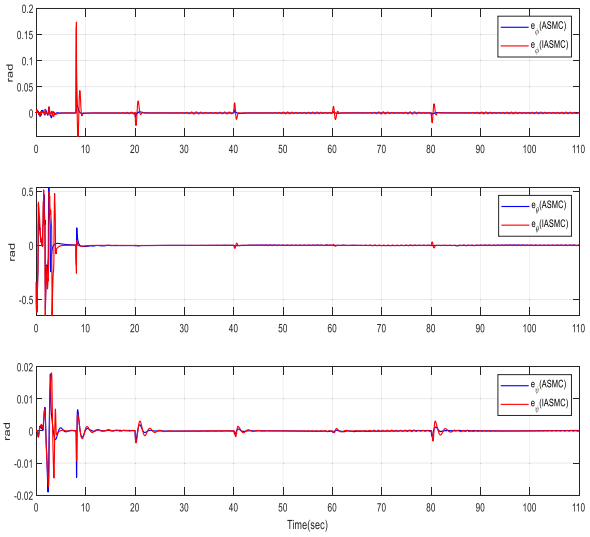

FIGURE 22. The error in the quadcopter attitude.

only increased when the state trajectory is away from the sliding surface (induced by the uncertainty) and decreased when the state trajectory approached the sliding surface.

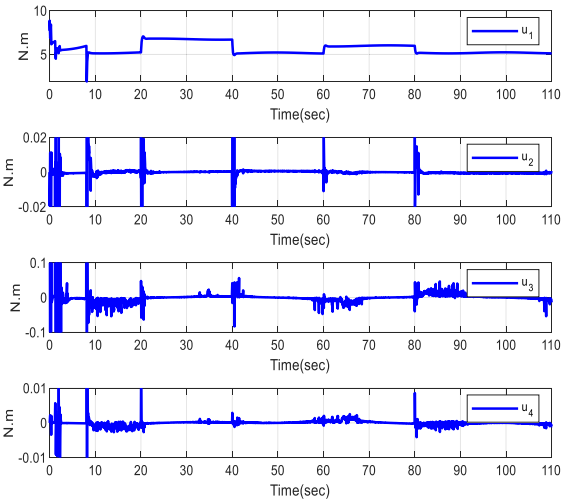

FIGURE 23. The control signals of the quadcopter with a constant switching gain.

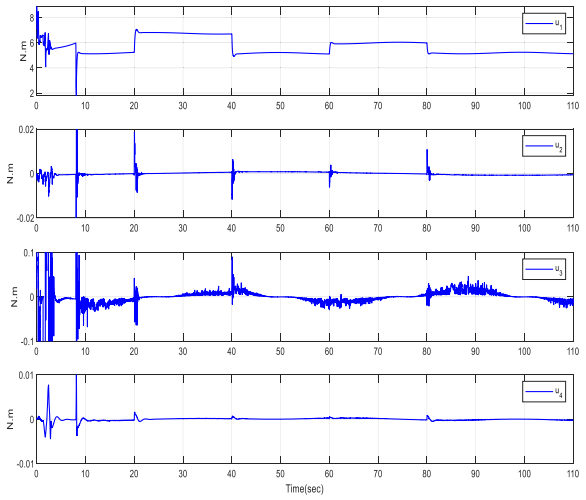

FIGURE 24. The control signals of the quadcopter with the ASMC controller.

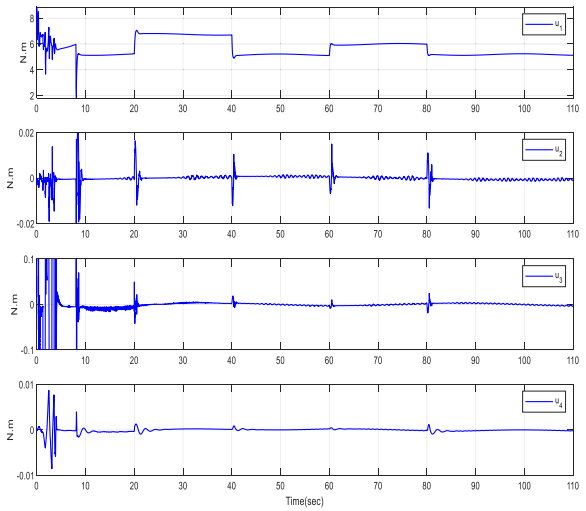

FIGURE 25. The control signals of the quadcopter with the IASMC controller.

This mechanism significantly contributed to the chattering attenuation.

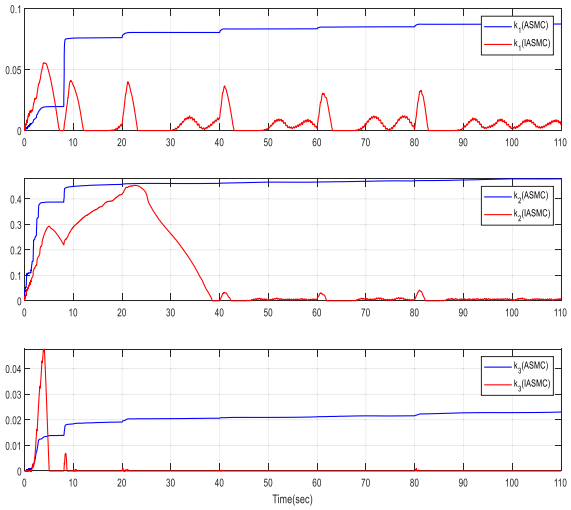

FIGURE 26. The switching gains for ASMC & IASMC.

VI. CONCLUSION

In this paper, the dynamic of a quadcopter has been divided into two subsystems, the attitude, and the position subsystems. The IASMC control has been proposed as an inner loop controller to control the quadcopter's attitude. The IT2-FPID controller has been proposed as an outer loop controller to control the quadcopter's position and generates the desired attitude to the inner loop proposed controller. The major drawback of the classical SMC control is the chattering phenomena, which is induced by the parameter uncertainties and unknown disturbance. The objective of this work is to design IASMC as an inner loop controller in order to attenuate the influence of the chattering in the presence of unbounded unknown uncertainties and unknown disturbances. Finally, the proposed IASMC scheme is simulated using a Matlab/Simulink platform and resulted in significant performance enhancement in terms of chattering attenuation and robust trajectory tracking. The proposed IASMC shows a remarkable performance in terms of chattering attenuation and trajectory tracking. However, there are many parameters in the control law that need to be tuned. These parameters can be optimized using a proper optimization algorithm with a suitable performance metric which will be considered in the future work.

REFERENCES

[1] L. R. García Carrillo, A. E. Dzul López, R. Lozano, and C. Pégard, "Quad Rotorcraft Control," *J. Universal Comput. Sci.*, vol. 9, no. 4, pp. 368–396, 2013.

[2] Y. Shtessel, C. Edwards, L. Fridman, and A. Levant, *Sliding Mode Control and Observation*. New York, NY, USA: Springer, 2014.

[3] S. Vaidyanathan and C. H. Lien, *Applications of Sliding Mode Control in Science and Engineering*, vol. 709. Cham, Switzerland: Springer, 2017.

[4] A. Noordin, M. A. M. Basri, and Z. Mohamed, "Sliding mode control for altitude and attitude stabilization of quadrotor UAV with external disturbance," *Indonesian J. Elect. Eng. Inform.*, vol. 7, no. 2, pp. 203–210, 2019.

[5] E. Kuantama, I. Tarca, and R. Tarca, "Feedback linearization LQR control for quadcopter position tracking," in *Proc. 5th Int. Conf. Control, Decis. Inf. Technol. (CoDIT)*, Apr. 2018, pp. 204–209.

[6] J. C. Escobar, R. Lozano, and M. B. Estrada, "PVTOL control using feedback linearisation with dynamic extension," *Int. J. Control*, 2019.

[7] O. Mofid and S. Mobayen, "Adaptive sliding mode control for finite-time stability of quad-rotor UAVs with parametric uncertainties," *ISA Trans.*, vol. 72, pp. 1–14, Jan. 2018.

[8] S. Nadda and A. Swarup, "On adaptive sliding mode control for improved quadrotor tracking," *J. Vib. Control*, vol. 24, no. 14, pp. 3219–3230, 2018.

[9] D. Lee, H. J. Kim, and S. Sastry, "Feedback linearization vs. Adaptive sliding mode control for a quadrotor helicopter," *Int. J. Control, Autom. Syst.*, vol. 7, no. 3, pp. 419–428, Jun. 2009.

[10] K. Mei and S. Ding, "Second-order sliding mode controller design subject to an upper-triangular structure," *IEEE Trans. Syst., Man, Cybern. Syst.*, early access, Nov. 5, 2018, doi: 10.1109/TSMC.2018.2875267.

[11] Q. Hou, S. Ding, and X. Yu, "Composite super-twisting sliding mode control design for PMSM speed regulation problem based on a novel disturbance observer," *IEEE Trans. Energy Convers.*, early access, Apr. 6, 2020, doi: 10.1109/TEC.2020.2985054.

[12] L. Liu, W. X. Zheng, and S. Ding, "High-order sliding mode controller design subject to lower-triangular nonlinearity and its application to robotic system," *J. Franklin Inst.*, vol. 357, no. 15, pp. 10367–10386, Oct. 2020.

[13] A. T. Nguyen and N. Xuan-mung, "Quadcopter adaptive trajectory tracking control: A new approach via backstepping technique," *Appl. Sci.*, vol. 9, no. 18, p. 3873, 2019.

[14] M. A. M. Basri, "Robust backstepping controller design with a fuzzy compensator for autonomous hovering quadrotor UAV," *Iranian J. Sci. Technol., Trans. Electr. Eng.*, vol. 42, no. 3, pp. 379–391, Sep. 2018.

[15] A. Mazinan, M. Kazemi, and H. Shirzad, "An efficient robust adaptive sliding mode control approach with its application to secure communications in the presence of uncertainties, external disturbance and unknown parameters," *Trans. Inst. Meas. Control*, vol. 36, no. 2, pp. 164–174, Apr. 2014.

[16] J. Zhu and K. Khayati, "A new approach for adaptive sliding mode control: Integral/exponential gain law," *Trans. Inst. Meas. Control*, vol. 38, no. 4, pp. 385–394, Apr. 2016.

[17] I. M. Boiko, "Chattering in sliding mode control systems with boundary layer approximation of discontinuous control," *Int. J. Syst. Sci.*, vol. 44, no. 6, pp. 1126–1133, Jun. 2013.

[18] H. Nemati, M. Bando, and S. Hokamoto, "Chattering attenuation sliding mode approach for nonlinear systems," *Asian J. Control*, vol. 19, no. 4, pp. 1519–1531, 2017.

[19] M. Labbadi, M. Cherkaoui, Y. El, and M. Guisser, "Modeling and robust integral sliding mode control for a quadrotor unmanned aerial vehicle," in *Proc. 6th Int. Renew. Sustain. Energy Conf. (IRSEC)*, Dec. 2018, pp. 1–6.

[20] O. Barambones and P. Alkorta, "Position control of the induction motor using an adaptive sliding-mode controller and observers," *IEEE Trans. Ind. Electron.*, vol. 61, no. 12, pp. 6556–6565, Dec. 2014.

[21] S. Di Gennaro, J. Rivera Dominguez, and M. A. Meza, "Sensorless high order sliding mode control of induction motors with core loss," *IEEE Trans. Ind. Electron.*, vol. 61, no. 6, pp. 2678–2689, Jun. 2014.

[22] A. Eltayeb, M. F. Rahmat, M. A. Mohammed Eltoum, and M. A. Mohd Basri, "Adaptive fuzzy gain scheduling sliding mode control for quadrotor UAV systems," in *Proc. 8th Int. Conf. Model. Simul. Appl. Optim. (ICMSAO)*, Apr. 2019, pp. 1–5.

[23] Y. Yang and Y. Yan, "Attitude regulation for unmanned quadrotors using adaptive fuzzy gain-scheduling sliding mode control," *Aerosp. Sci. Technol.*, vol. 54, pp. 208–217, Jul. 2016.

[24] N. Ben, S. Bouallègue, and J. Haggège, "Fuzzy gains-scheduling of an integral sliding mode controller for a quadrotor unmanned aerial vehicle," *Int. J. Adv. Comput. Sci. Appl.*, vol. 9, no. 3, pp. 132–141, 2018.

[25] E. Ahmed, "Robust adaptive sliding mode control design for quadrotor unmanned aerial vehicle trajectory tracking," *Int. J. Comput. Digit. Syst.*, vol. 9, no. 2, pp. 249–257, Jan. 2020.

[26] J. Soltani and M. M. Rezaei, "Robust control of an islanded multi-bus microgrid based on input–output feedback linearisation and sliding mode control," *IET Gener., Transmiss. Distrib.*, vol. 9, no. 15, pp. 2447–2454, 2015.

[27] A. Eltayeb, M. F. Rahmat, M. A. M. Eltoum, S. Ibrahim, and M. A. M. Basri, "Adaptive sliding mode control design for the 2-DOF robot arm manipulators," in *Proc. Int. Conf. Comput., Control, Electr., Electron. Eng. (ICCCEEE)*, Sep. 2019, pp. 1–5.

[28] J. Baek, M. Jin, and S. Han, "A new adaptive sliding-mode control scheme for application to robot manipulators," *IEEE Trans. Ind. Electron.*, vol. 63, no. 6, pp. 3628–3637, Jun. 2016.

[29] Q. Quan, *Introduction to Multicopter Design and Control*. Beijing, China: Springer, 2017.

[30] A. Eltayeb, M. F. Rahmat, and M. A. M. Basri, "Adaptive feedback linearization controller for stabilization of quadrotor UAV," *Int. J. Integr. Eng.*, vol. 12, no. 4, pp. 1–17, 2020.
[31] A. Eltayeb, M. F. Rahmat, M. A. M. Basri, and M. S. Mahmoud, "An improved design of integral sliding mode controller for chattering attenuation and trajectory tracking of the quadrotor UAV," *Arabian J. Sci. Eng.*, vol. 45, no. 8, pp. 6949–6961, Aug. 2020.
[32] R. Olfati-Saber, "Nonlinear control of underactuated mechanical systems with application to robotics and aerospace vehicles," Ph.D. dissertation, Massachusetts Inst. Technol., Cambridge, MA, USA, 2001.
[33] H. Boudjedir, O. Bouhali, and N. Rizoug, "Adaptive neural network control based on neural observer for quadrotor unmanned aerial vehicle," *Adv. Robot.*, vol. 28, no. 17, pp. 1151–1164, Sep. 2014.
[34] Z. Li, X. Ma, and Y. Li, "Model-free control of a quadrotor using adaptive proportional derivative-sliding mode control and robust integral of the signum of the error," *Int. J. Adv. Robotic Syst.*, vol. 15, no. 5, pp. 1–15, 2018.
[35] O. Castillo, L. Amador-Angulo, J. R. Castro, and M. Garcia-Valdez, "A comparative study of type-1 fuzzy logic systems, interval type-2 fuzzy logic systems and generalized type-2 fuzzy logic systems in control problems," *Inf. Sci.*, vol. 354, pp. 257–274, Aug. 2016.
[36] O. Castillo, "Introduction to type-2 fuzzy logic control," in *Type-2 Fuzzy Logic in Intelligent Control Applications*. Berlin, Germany: Springer, 2012, pp. 3–5.
[37] G. Ruiz-Garcia, H. Hagras, H. Pomares, and I. R. Ruiz, "Toward a fuzzy logic system based on general forms of interval Type-2 fuzzy sets," *IEEE Trans. Fuzzy Syst.*, vol. 27, no. 12, pp. 2381–2395, Dec. 2019.
[38] A. Sarabakha, C. Fu, E. Kayacan, and T. Kumbasar, "Type-2 fuzzy logic controllers made even simpler: From design to deployment for UAVs," *IEEE Trans. Ind. Electron.*, vol. 65, no. 6, pp. 5069–5077, Jun. 2018.
[39] J. M. Mendel, H. Hagras, W. W. Tan, W. W. Melek, and H. Ying, *Introduction To Type-2 Fuzzy Logic Control: Theory and Applications*, vol. 9781118278. New York, NY, USA: Wiley, 2014.
[40] S. Bouabdallah, "Design and control of quadrotors with application to autonomous flying," Ph.D. dissertation, EPFL, Lausanne, Switzerland, 2007.

AHMED ELTAYEB received the B.S. degree in electronic engineering from the University of Gezira, Sudan, in 2008, and the M.Sc. degree in systems engineering from the King Fahd University of Petroleum and Minerals, Saudi Arabia, in 2013. He is currently pursuing the Ph.D. degree with the Division of Control and Mechatronics Engineering, UTM University, Malaysia. He was appointed as a Teaching Assistant with the Department of Electronic Engineering, University of Gezira, from 2008 to 2010. He was appointed as a Researcher Assistant with the Department of Systems Engineering, KFUPM University. His research interests include robotics and unmanned aerial vehicles control design.

MOHD FUA'AD RAHMAT (Senior Member, IEEE) received the B.E.Eng. degree (Hons.) from Universiti Teknologi Malaysia (UTM), Skudai Johor, in 1989, and the master's degree in control system engineering from The University of Sheffield, U.K., in 1993, and the Ph.D. degree in electronic instrumentation engineering from Sheffield Hallam University, U.K., in 1996. In 1990, he appointed as an Assistant Lecturer A with UTM, where he is currently a Professor with the Department of Control and Mechatronics Engineering, Faculty of Electrical Engineering. His research interests include system identification and estimation, signal processing, process tomography for industrial process, process control instrumentation, sensors and actuators, hydraulic, and pneumatic systems.

MOHD ARIFFANAN MOHD BASRI received the B.Eng. degree in electrical–mechatronics, the M.Eng. degree in electrical–mechatronics and automatic control, and the Ph.D. degree in electrical–control from Universiti Teknologi Malaysia (UTM), Johor Bahru, Malaysia, in 2004, 2009, and 2015, respectively. He is currently a Senior Lecturer with the School of Electrical Engineering, Faculty of Engineering, UTM. He has authored more than 30 journal and conference papers, and book chapters. His current research interests include advanced control techniques, artificial intelligent, and their applications. He is a member of the Board of Engineers Malaysia (BEM), the Malaysia Board of Technologists (MBOT), the Malaysian Society for Automatic Control Engineers (MACE), the Malaysian Simulation Society (MSS), and the International Association of Engineers (IAENG).

M.A MOHAMMED ELTOUM received the B.S. degree in electrical engineering from the Sudan University of Science and Technology, Sudan, in 2015, and the master's degree in systems and control engineering from the King Fahd University of Petroleum and Minerals, Saudi Arabia, in 2020. His research interests include nonlinear control systems, electric drives, mechatronics, and intelligent control systems.

SAMI EL-FERIK received the B.Sc. degree in electrical engineering from Laval University, Quebec, QC, Canada, and the M.S. and Ph.D. degrees in electrical and computer engineering from Ecole Polytechnique, University of Montreal, Montreal, QC, Canada. His Ph.D. work, on flexible manufacturing systems modeling and control, was co-supervised with Mechanical Engineering. After completion of his Ph.D. and Postdoctoral positions, he worked with Pratt and Whitney Canada as a Staff Control Analyst at the Research and Development Center of Systems, Controls, and Accessories. He is currently an Associate Professor in Control and Instrumentation with the Department of Systems Engineering, KFUPM. His research interests include sensing, monitoring, and control with strong multidisciplinary research and applications. His research contributions are in control of drug administration, process control, and control loop performance monitoring, control of systems with delays, modeling and control of stochastic systems, analysis of network stability, condition monitoring, and condition-based maintenance.